A study of the magnetic critical scattering from $FeCO_3$ by time-of-flight neutron diffraction

1996 J. Phys.: Condens. Matter 8 91

(http://iopscience.iop.org/0953-8984/8/1/010)

J. Phys.: Condens. Matter **8** (1996) 91–100. Printed in the UK

A study of the magnetic critical scattering from $FeCO_3$ by time-of-flight neutron diffraction

S J Payne†, M E Hagen† and M J Harris‡

† Department of Physics, Keele University, Keele, Staffordshire ST5 5BG, UK

‡ Rutherford Appleton Laboratory, Chilton, Didcot, Oxfordshire OX11 0QX, UK

Received 16 August 1995, in final form 31 October 1995

Abstract. The temperature dependences of the magnetic critical scattering above T_N and the staggered magnetization below T_N have been measured for the antiferromagnet $FeCO_3$ using time-of-flight neutron diffraction techniques. $FeCO_3$ undergoes a paramagnetic to antiferromagnetic phase transition at its Néel temperature and was expected to be characterized by the universality class of the $d = 3$ Ising model. The transition, which occurs at $T_N = 37.77 \pm 0.02$ K, appears to be that of a continuous second-order transition. From an analysis of the critical scattering data, the exponents $\nu = 0.61 \pm 0.03$ and $\gamma = 1.17 \pm 0.06$ have been deduced. These values are in general agreement with the theoretical values for the $d = 3$ Ising model of $\nu = 0.63$ and $\gamma = 1.24$. From the temperature dependence of the staggered magnetization below T_N the exponent $\beta = 0.32 \pm 0.01$ has been determined, which is also consistent with the theoretical value of $\beta = 0.33$ for the $d = 3$ Ising model.

1. Introduction

Iron carbonate is a naturally occurring mineral commonly known as *siderite*, and has a rhombohedral crystal structure belonging to the space group $R\bar{3}c$ with two molecules per unit cell [1]. Previous neutron diffraction studies carried out on $FeCO_3$ have shown [2, 3] that the magnetic Fe^{2+} ions order antiferromagnetically at a temperature of $\approx$38 K in alternating (001) ferromagnetic sheets with their spins directed along the hexagonal c-axis. Inelastic neutron scattering measurements by Wrege *et al* [2] have shown that the spin-wave dispersion relations in $FeCO_3$ are essentially flat with an energy gap of $\sim$13 meV. This large spin-wave gap is due to the strong uniaxial crystal-field anisotropy in $FeCO_3$ [4] and it is this large uniaxial anisotropy which leads to the expectation that $FeCO_3$ should belong to the universality class of the $d = 3$ Ising model.

In this paper we report the results of time-of-flight neutron diffraction measurements of the magnetic critical scattering associated with the paramagnetic to antiferromagnetic phase transition in $FeCO_3$. We also report results for the temperature dependence of the staggered magnetization in the critical region. This is the first time that the time-of-flight technique has been used to measure magnetic critical scattering and the choice of material for study in this case was made for a number of reasons. Firstly, as mentioned above, the transition in $FeCO_3$ was expected to belong to a reasonably simple and well known class of transitions, that of the $d = 3$ Ising model. Secondly this carbonate compound is one of a family of carbonate and nitrate compounds whose properties have been of great interest in recent years [5]. Thirdly, previous studies of antiferromagnets in the $d = 3$ Ising class have been carried out on materials with the high-symmetry tetragonal crystal structure (see,

0953-8984/96/010091+10$19.50

for example, the reviews in [6, 7]) and we were interested to see whether or not the $d = 3$ Ising model would work as well for a material with the lower-symmetry rhombohedral structure [3] such as $FeCO_3$.

2. Experimental details

The neutron diffraction measurements were carried out on a natural single crystal of $FeCO_3$ using the PRISMA spectrometer at the ISIS Spallation Neutron Source, Rutherford Appleton Laboratory, UK. In the work reported in this paper PRISMA was operated as a multi-detector single-crystal diffractometer with Soller collimation in front of each of the detectors in the detector bank. This was achieved by removing the analyser crystals and allowing the detectors to each view the sample directly through their individual collimators.

A natural single crystal of $FeCO_3$ was used because it is not possible to grow artificial single crystals of $FeCO_3$ large enough for neutron scattering studies [8]. As a consequence siderite, like many naturally occurring minerals, can contain substantial amounts of impurities. For the studies on the crystal reported here the presence of scattering due to impurities was evident, although the amount was small and not a major problem in analysing the results obtained for the critical scattering. The sample used had a volume of ~ 2 cm^3 and was oriented so that the $(H, 0, 0)$ and $(0, 0, L)$ reciprocal-lattice vectors were in the scattering plane. It was cemented to the preshaped end of an aluminium peg which was mounted in an aluminium sample can. The peg and cement were masked off with Gd foil and thin Cd metal sheet to avoid any background scattering which might arise from them.

The sample can was attached to the copper block assembly of a closed-cycle refrigerator which was used to control the sample temperature. In order to ensure that the crystal was in good thermal contact with its surroundings the sample can was filled with helium gas to act as a temperature exchange medium. The temperature of the sample was measured with a platinum resistance thermometer inside the sample can, which was read and recorded every 30 seconds by the spectrometer control computer during the data collection. This temperature readout was used to determine the mean sample temperature for a particular run and also its stability. The latter was found to be ± 0.03 K or better for periods of up to six hours while the data were being taken.

Since the crystallographic and magnetic structures of $FeCO_3$ are such that nuclear and magnetic neutron scattering occur at the same Bragg peak wavevector positions in reciprocal space [3], it was necessary to measure the magnetic critical scattering at a reciprocal-lattice position where the nuclear structure factor is zero. Although in the $R\bar{3}c$ structure the $(0, 0, L)$ Bragg peak positions with $L = 3 + 6n$ are well known to have a zero nuclear structure factor, in the case of $FeCO_3$ they also have a zero magnetic structure factor. This is because magnetic neutron scattering is only allowed for components of the magnetic moment perpendicular to the neutron wavevector transfer $\boldsymbol{Q}$ [7] and at these $(0, 0, L)$ positions $\boldsymbol{Q}$ is parallel to the magnetic moment. Therefore we chose to measure the magnetic critical scattering at the $(1, 0, 1)$ Bragg peak position (which is the $(1, 0, 0)$ position in rhombohedral coordinates) which also has a zero nuclear structure factor because of the c-glide plane in the $R\bar{3}c$ structure [3]. However, the magnetic structure factor for the $(1, 0, 1)$ Bragg peak wavevector is non-zero because $\boldsymbol{Q}$ is at $\sim 76^\circ$ to the $(0, 0, L)$ axis, i.e. the direction of the magnetic moments. An added advantage of measuring at the $(1, 0, 1)$ wavevector is that it is also the magnetic Bragg peak position which has the smallest $|\boldsymbol{Q}|$, and therefore its intensity is least attenuated by the effect of the form factor for magnetic neutron scattering [7].

The PRISMA spectrometer has a white incident neutron beam which means that it is

possible to select any scattering angle ϕ at which to measure the (1, 0, 1) Bragg peak, since there is always a wavelength available in the incident beam to satisfy Bragg's law. In the experiment reported here ϕ-angles in the range from -46° to -40° were used. Since $FeCO_3$ is very Ising-like, the energy width of the critical scattering is narrow and this means that even relatively low incident neutron energies can be used to integrate over this energy width and still satisfy the quasi-static approximation [6, 7]. It should be noted that the quasi-static approximation is satisfied by essentially the same criteria for time-of-flight measurements [10, 11] as it is for continuous neutron beam measurements [12]. The use of low-energy incident neutrons, which still satisfy the quasi-static approximation, gives the added advantage of a better wavevector resolution.

Another important factor when choosing a suitable ϕ-angle for a measurement is to select one that avoids the possible occurrence of multiple scattering [6]. Although there is no nuclear Bragg peak at the (1, 0, 1) position, we found experimentally that for neutron energies in the range 13.8 meV to 19.6 meV (i.e. ϕ-angles from -36° to -30°) multiple scattering can, falsely, indicate the presence of a nuclear Bragg peak at the (1, 0, 1) position. However, measurements showed that for ϕ-angles less than -40° this was not a problem.

3. Results

The results of our measurements on $FeCO_3$ are given in the following subsections. Firstly, in subsection 3.1, the results from the Bragg peak intensity measurements below T_N are reported along with the value of the β-exponent deduced from them. In subsection 3.2 we describe how the critical scattering above T_N was collected and transformed and then in subsection 3.3 how it was analysed in order to extract values for the staggered susceptibility and inverse correlation lengths. Subsection 3.4 reports on the fitting procedure used to obtain the critical exponents ν_c, ν_{ab} and γ from these values.

3.1. Magnetic Bragg peak data (T below T_N)

The measurements of the temperature dependence of the magnetic Bragg peak were made using a single detector which was set at a ϕ-angle of -40° with respect to the incident neutron beam. In order to obtain the integrated Bragg peak intensity the rotation angle of the crystal was stepped through its peak position and a time-of-flight spectrum collected at each step. These rocking curve scans were performed for a number of temperatures ranging from 36.58 K up to 38.52 K (just beyond the expected transition temperature of $\sim$38 K). The data in each radial scan were integrated over a restricted time-of-flight range around the flight time corresponding to the (1, 0, 1) Bragg peak and the resulting data points were then integrated over the rocking curve angle.

The values of the integrated intensity obtained were then fitted, as a function of temperature, to the power-law equation

$$I(T) = I_0 t^{2\beta} \tag{1}$$

where t is the reduced temperature ($t = |T - T_N|/T_N$). From this fitting procedure, values for the Néel temperature T_N and the critical exponent β were obtained. The 18 data points obtained from the integrated intensities of the rocking curves over the temperature range 36.58 to 38.52 K are shown in figure 1 as a function of temperature. The data points in the temperature range from 36.58 to 37.70 K result from the magnetic Bragg peak alone and the flatter band of scattering over the range of temperatures from 37.87 to 38.52 K is due to the weaker critical scattering. From the position of the data point at 37.74 K it is

not clear how much of the scattering is due to the Bragg peak and how much to the critical scattering. Therefore the next-lowest temperature, 37.70 K, was chosen as the upper limit for the temperatures used in the fitting of the magnetic Bragg peak data in order to avoid any effects from the critical scattering.

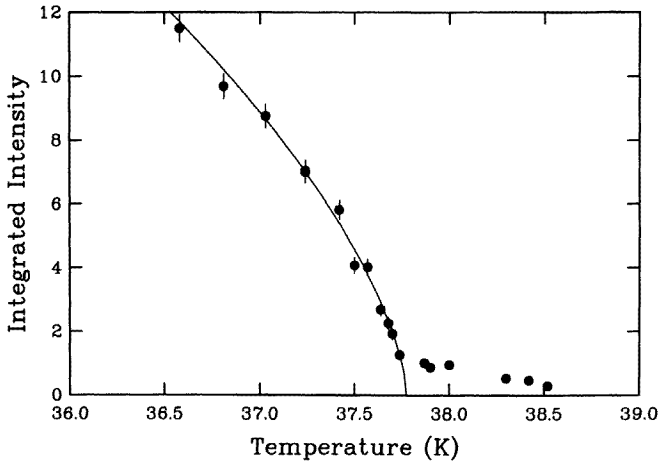

Figure 1. The integrated intensity of the (1, 0, 1) magnetic Bragg peak data against temperature in the range 36.58 K to 38.52 K.

The fitting procedure was performed twice; the first time I_0, T_N and 2β were allowed to vary and the second time T_N was fixed at a weighted average value obtained from the results of the first Bragg peak fit and the values for the transition temperature produced from the fits to the critical scattering data, which are discussed in section 3.2. Table 1 shows the results obtained from the two fits to the magnetic Bragg peak data. It can be seen that the values for 2β in both cases are in reasonable agreement with the value expected for the $d = 3$ Ising model of $2\beta = 0.63$ [7]. The solid line shown in figure 1 is the result for $I(T)$ calculated using the values obtained from the second fit with T_N fixed.

Table 1. The values found from fitting the integrated intensity of the (1, 0, 1) magnetic Bragg peak to the equation $I(T) = I_0 t^{2\beta}$ as described in the text.

	Amplitude	2β	T_N
Free fit	94 ± 17	0.61 ± 0.05	37.76 ± 0.02
T_N fixed	105 ± 9	0.64 ± 0.02	37.77

A problem that affects any attempt to measure the β-exponent using neutron scattering is that of primary extinction [6, 11], which occurs when the scattering strength of a Bragg peak is so strong that the neutron beam does not fully penetrate into the crystal. For a measurement of the β-exponent the complexity is that the Bragg intensity (scattering strength) is highly temperature dependent, being essentially zero at T_N but very strong at lower temperatures. Hence any primary extinction effects will also depend upon temperature and can therefore potentially change the temperature dependence of the observed Bragg peak intensity and hence invalidate the determination of β from equation (1). Since in the work reported here the data we have used to obtain β were limited to a temperature range which

was not more than ∼1.2 K below T_N (i.e. a reduced temperature $|t| < 0.03$), where the Bragg peak remains relatively weak, it is hoped that primary extinction was not a problem.

3.2. Magnetic critical scattering data (T above T_N)

The critical scattering data above T_N were collected using four detectors that were positioned with ϕ-angles of -46°, -44°, -42° and -40° respectively. This configuration allowed an appropriate range of incident neutron energies to be selected which took into consideration resolution effects, the quasi-static approximation and the problems of multiple scattering. The use of four detectors allowed the simultaneous collection of four radial time-of-flight scans through the magnetic critical scattering peak. However, in order to cover the whole area of the critical scattering in reciprocal space in more detail, further radial scans were required. This was achieved by stepping the rotation angle of the crystal through a set of 12 angles in a 20° range centred on the angle for the (1, 0, 1) Bragg peak. These 12 steps produced a total of 48 radial time-of-flight scans.

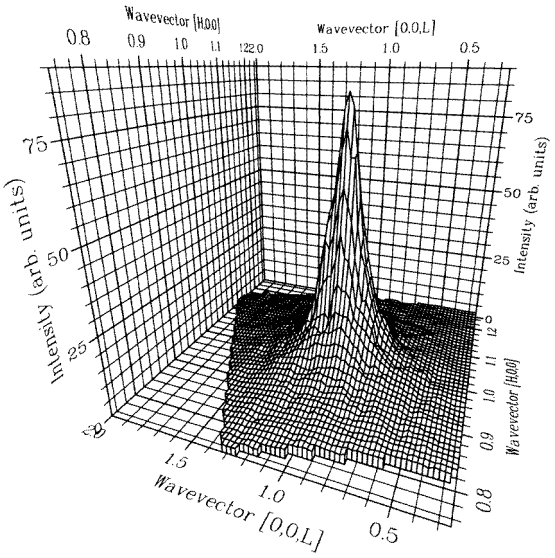

Figure 2. A surface grid plot of the critical scattering measured at 38.10 K.

These raw time-of-flight scans through the critical scattering around the (1, 0, 1) position were transformed using the program VCRS [9] into reciprocal-lattice coordinates for 71 steps in the wavevector transfer range from 1.25 $Å^{-1}$ to 1.95 $Å^{-1}$ (the (1, 0, 1) Bragg peak has a wavevector transfer of 1.5935 $Å^{-1}$). This program also normalizes the data for the energy dependence of the incident neutron flux using the monitor spectrum, compensates for the variation of the monitor efficiency with energy and normalizes the data among different detectors using a vanadium calibration spectrum. When taken together the 71 data points in each of the 48 radial scans in reciprocal space effectively form a grid of ∼3400 points mapping out the critical scattering. In figure 2 we show a surface plot of the measured grid of critical scattering from $FeCO_3$ at 38.10 K.

3.3. Analysis of the critical scattering data

In order to extract the staggered susceptibility and the inverse correlation lengths the grid of data was fitted to a lineshape for the critical scattering. Each of the data points in the grid is the result of a convolution of the structure factor $S(\boldsymbol{Q})$ for the critical scattering, which was centred at the $(1, 0, 1)$ position, with the resolution function of the PRISMA spectrometer, centred at that particular data point. The structure factor $S(\boldsymbol{Q})$ used in the analysis was modelled by a Lorentzian function given by

$$S(\boldsymbol{Q}) = \chi_0 \Big/ \left\{ 1 + \left(\frac{Q_L - Q_L^0}{\kappa_c} \right)^2 + \left[\frac{(Q_H - Q_H^0)^2 + Q_V^2}{\kappa_{ab}^2} \right] \right\} \tag{2}$$

where Q_L, Q_H and Q_V represent, respectively, the wavevector components along the $(0, 0, L)$ and $(H, 0, 0)$ directions in the scattering plane, and vertically out of the scattering plane. An allowance has been made in equation (2) for the inverse correlation lengths along the c-axis (κ_c) and perpendicular to the c-axis, in the a–b plane (κ_{ab}) to be different. Although theoretically these inverse correlation lengths should have the same temperature dependence and hence the same critical exponent ν, they can have different critical amplitudes. The Lorentzian function is centred on the position $Q_L^0 = 1$ and $Q_H^0 = 1$ and its height, χ_0, is equal to the isothermal staggered susceptibility. The resolution function used was essentially that described in appendix B of the paper by Hagen and Steigenberger [13], with some slight modifications which are described in appendix A of this paper.

As briefly discussed in section 2, since a natural crystal was used there were impurities in the sample. This led to a small extra peak at the position $(1.018, 0, 1.035)$. At temperatures far above T_N this peak is distinct from the broad critical scattering while close to T_N it is overshadowed by the intensity of the critical scattering. This peak was modelled in the data analysis by a Gaussian function with radial and transverse full widths at half maxima of 0.021 Å^{-1} and 0.030 Å^{-1} respectively. These values and also the height of the Gaussian were found from the high-temperature data sets where the peak was distinct and were held fixed at other temperatures.

The fitting involved minimizing the least-squares agreement factor A [14] given by

$$A = \sqrt{\frac{1}{N-k} \sum_{i=1}^{N} \left(\frac{I_i^{obs} - I_i^{cal}}{\sigma_i} \right)^2} \tag{3}$$

where N is the number of data points, k is the number of adjustable parameters, I_i^{obs} and I_i^{cal} are the experimentally observed and calculated intensities and σ_i the (standard deviation) error in the observed intensity. This procedure was carried out using the program CRTFIT [11] which minimized A using a Marquardt method [14] and evaluated the convolution integrals leading to the calculated values by an importance-sampling Monte Carlo method. The best-fit agreement factors ranged in value from 0.96 to 1.10. An examination was also made of the grid maps of the residuals [11] corresponding to the best-fit results to ensure that there were no unreasonable correlations between the residuals. In figures 3(a), 3(b) and 3(c) we show some radial cuts through the grids of experimental data at temperatures of (a) 38.10 K, (b) 38.92 K and (c) 40.66 K. The solid lines in these figures are the same radial cuts through the grid of best-fit calculated values. These cuts follow the path $[H, 0, 1.017H]$ rather the path $[H, 0, H]$ so they display the impurity peak as well as the critical scattering. At the highest temperature of 40.66 K (figure 3(c)) the impurity peak can be clearly seen as separate from the critical scattering.

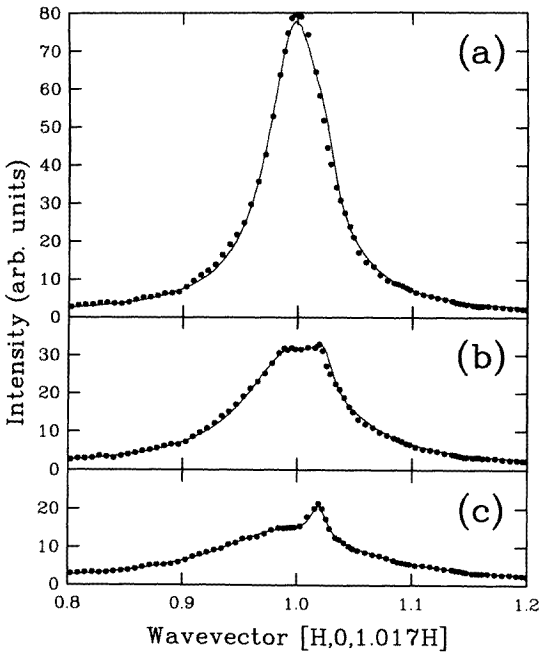

Figure 3. Radial cuts through the grid of critical scattering data which pass through the impurity peak at temperatures of (a) 38.10 K, (b) 38.92 K and (c) 40.66 K.

3.4. Critical scattering exponent values

The values of κ and χ_0 deduced from fitting the critical scattering lineshapes are shown in figures 4(a) and 4(b). These values were fitted to the power-law equations

$$\kappa_c = \kappa_c^0 t^{\nu_c} \tag{4}$$

$$\kappa_{ab} = \kappa_{ab}^0 t^{\nu_{ab}} \tag{5}$$

$$\chi_0 = \chi_0^0 t^{-\gamma} \tag{6}$$

where t is the reduced temperature, in order to extract the critical exponents ν and γ. Initially these fits were performed with the transition temperature T_N as an adjustable parameter in each case. However, because the values for T_N were all very similar and also similar to the value found from fitting the Bragg peak intensities, the fits were repeated with T_N fixed at a weighted average value. In table 2 the results of all of these free and fixed fits are given and in figures 4(a) and 4(b) the solid lines are the results of the fits with T_N fixed.

Table 2. The results for the critical exponents ν_c, ν_{ab} and γ obtained from fitting the values for κ_c, κ_{ab} and χ_0.

	Exponent	Amplitude	T_N (K)
χ_0	$\gamma = 1.11 \pm 0.13$	0.13 ± 0.01	37.81 ± 0.02
(with T_N fixed)	$\gamma = 1.17 \pm 0.06$	0.11 ± 0.01	37.77
κ_c	$\nu_c = 0.61 \pm 0.03$	1.25 ± 0.11	37.77 ± 0.05
(with T_N fixed)	$\nu_c = 0.61 \pm 0.03$	1.25 ± 0.11	37.77
κ_{ab}	$\nu_{ab} = 0.60 \pm 0.03$	0.34 ± 0.03	37.78 ± 0.05
(with T_N fixed)	$\nu_{ab} = 0.61 \pm 0.03$	0.35 ± 0.03	37.77

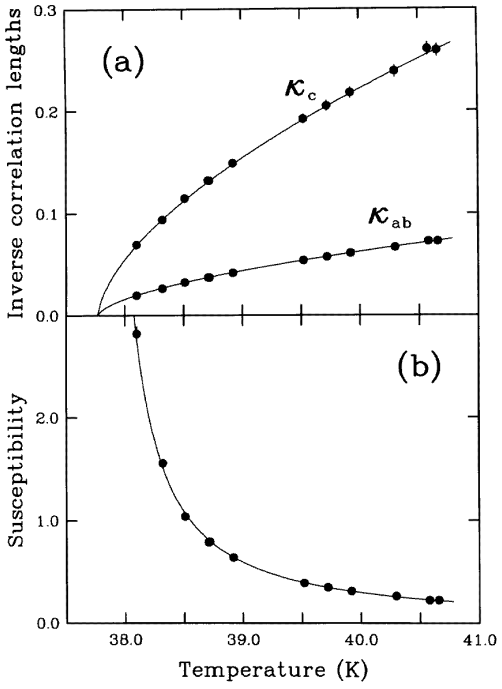

Figure 4. The temperature dependences of (a) the inverse correlation lengths κ_c and κ_{ab}, and (b) the isothermal staggered susceptibility χ_0 are shown. The solid lines are the best-fit results for the power-law equations (4) to (6) as described in the text.

It can be seen from table 2 that, in agreement with theory, ν_c and ν_{ab} are the same within error. The average value for ν of 0.61 ± 0.03 agrees, within error, with the theoretical value for the $d = 3$ Ising model of 0.63. The value obtained for γ of 1.17 ± 0.06 was on the low side of the theoretical value of 1.24 although it is still in reasonable agreement with this value. The exponent β obtained from the magnetic Bragg peak data was, as can be seen in table 1, in slightly better agreement with theory than either ν or γ. It should be noted, however, that the Bragg peak data were taken over a reduced temperature range which was closer to T_N than that of the critical scattering data.

4. Discussion

The experimental work reported here had essentially two aims, to develop a technique for carrying out critical scattering measurements at a pulsed neutron source and to examine whether the $d = 3$ Ising model was appropriate for the antiferromagnetic phase transition in rhombohedral $FeCO_3$. The results reported here are essentially in agreement with the $d = 3$ Ising model, certainly for the Bragg peak data below the transition temperature. For the critical scattering data collected above T_N there is reasonable agreement between theory and experiment although better agreement with the theoretical values would probably have been achieved if data could have been taken at temperatures closer to the transition temperature. However, this would have required better resolution and the limiting factor in the resolution function was the mosaic spread of the natural crystal. It was not possible to obtain a natural crystal with a smaller mosaic spread than the one we used and since synthetic crystals of a reasonable size cannot be grown at this time higher-resolution measurements are unattainable. Even so, comparing the values of ν and γ in table 2 with the theory values of 0.63 and 1.24 respectively, and taking into account the range of reduced temperatures, it

can be seen that these values are consistent with $FeCO_3$ belonging to the universality class of the $d = 3$ Ising model.

Acknowledgments

This work was supported by the United Kingdom Engineering and Physical Sciences Research Council under grant number GR/K-04989 and at the ISIS Facility. One of us (SJP) acknowledges the financial support of an EPSRC studentship and a CASE award from the Rutherford Appleton Laboratory. The crystal of $FeCO_3$ was kindly provided by the University Museum, University of Oxford.

Appendix A. The resolution function

The resolution function of a neutron diffractometer can be defined as the relative probability of observing a neutron with a wavevector transfer $\boldsymbol{Q}_0 + \Delta\boldsymbol{Q}$ when the instrument has been set to record a wavevector transfer $\boldsymbol{Q}_0$. The resolution function for the PRISMA spectrometer [13] differs slightly from that for the triple-axis spectrometer [15, 16] which has been widely used at continuous neutron sources for critical scattering measurements [7]. The principal difference is the asymmetric nature of the neutron pulse lineshape at a spallation source. The equation that we have used for the resolution function of the PRISMA spectrometer is

$$R(\boldsymbol{Q}) = \left(\frac{1}{V}\right)\exp\left[-\frac{1}{2}\left(\left(\frac{\Delta Q_T}{\sigma_{DT}}\right)^2 + \left(\frac{\Delta Q_V}{\sigma_{DV}}\right)^2\right)\right]\exp\left[-\frac{T^*}{\tau}\right]\operatorname{erfc}\left[\frac{1}{\sqrt{2}}\left(\frac{\sigma_0}{\tau} - \frac{T^*}{\sigma_0}\right)\right] \tag{A1}$$

where

$$\sigma_{DV} = \sqrt{(\sigma_{SV}\,Q_0)^2 + (k_0)^2\left(\sigma_{1V}^2 + \sigma_{EV}^2\right)} \tag{A2}$$

$$\frac{1}{\sigma_{EV}^2} = \frac{1}{\sigma_{2V}^2} + \frac{1}{\sigma_{3V}^2} \tag{A3}$$

$$\sigma_{DT} = \frac{1}{2}Q_0\sqrt{\sigma_{1H}^2 + \sigma_{EH}^2 + 4\sigma_{SH}^2} \tag{A4}$$

$$\frac{1}{\sigma_{EH}^2} = \frac{1}{\sigma_{2H}^2} + \frac{1}{\sigma_{3H}^2} \tag{A5}$$

$$\sigma_0 = \chi_0 \cot\left(\frac{|\phi|}{2}\right)\sqrt{\frac{\sigma_{1H}^2\sigma_{EH}^2 + \sigma_{1H}^2\sigma_{SH}^2 + \sigma_{EH}^2\sigma_{SH}^2}{\sigma_{1H}^2 + \sigma_{EH}^2 + 4\sigma_{SH}^2}} \tag{A6}$$

$$T^* = \left(\frac{\chi_0}{Q_0}\right)\left[\Delta Q_L + \frac{\sigma_{1H}^2 - \sigma_{EH}^2}{\sigma_{1H}^2 + \sigma_{EH}^2 + 4\sigma_{SH}^2}\cot\left(\frac{\phi}{2}\right)\Delta Q_T\right] \tag{A7}$$

$$\chi_0 = m_N\left(L_i + L_f\right)/\hbar k_0 \tag{A8}$$

$$V = \left(\frac{1}{\chi_0}\right)\sigma_{DV}\sigma_{DT}\tau\,Q_0\exp\left[-\frac{1}{2}\left(\frac{\sigma_0}{\tau}\right)^2\right]. \tag{A9}$$

This is essentially equation (B.6) from [13] and the notation that we have used is identical to that in [13]. The difference is that in equation (A1) the resolution function has been normalized by dividing by its volume V. In transforming the raw time-of-flight data to reciprocal-lattice units the intensities of the data were normalized to a vanadium calibration

spectrum [11]. This procedure is primarily followed to remove any difference in efficiency between the detectors used, but it also leads to the normalization of the resolution function by its volume.

Table A1. The relevant parameter values for the PRISMA spectrometer and the $FeCO_3$ crystal needed in the evaluation of the resolution function are given. The parameters f are the full width at half maximum values in degrees equivalent to the σ-values used in equations (A2) to (A9) which are standard deviations. The lattice parameters a and c refer to the hexagonal unit cell.

Flight path lengths		
$L_i = 9.035$ m	$L_f = 0.7595$ m	
Collimation parameters		
$f_{1H} = 0.25^\circ$	$f_{2H} = 0.87^\circ$	$f_{3H} = 0.87^\circ$
$f_{1V} = 0.42^\circ$	$f_{2V} = 3.10^\circ$	$f_{3V} = \infty$
Sample parameters		
$f_{SH} = 1.15^\circ$	$f_{SV} = 1.15^\circ$	
$a = 4.698$ Å	$c = 15.997$ Å	

The parameters used to describe the slowing-down time τ of the neutron pulse were as given in [13]. The full width at half maximum parameter values used for the collimation and sample mosaic spread are given in table A1. These values are related to the standard deviations σ used in equations (A2) to (A9) by the relation $\sigma = f/2.35$ and accurately reproduce the radial and rocking curve widths of the crystal Bragg peaks at various energies. However, it should be noted that because the crystal of $FeCO_3$ was a natural crystal it had a relatively large sample mosaic spread η_s, which tended to dominate the Bragg peak widths. Therefore in order to check the accuracy of all of our resolution function parameters, Bragg peak measurements were also carried out on an effectively perfect $LiNbO_3$ crystal (i.e. with $\eta_s \sim 0$). The collimation parameters given in table A1 accurately reproduced the Bragg peak measurements on this crystal as well.

References

[1] Zhou Yi-Yang and Yin Chun-Hao 1993 *Phys. Rev.* B **47** 5451
[2] Wrege D E, Spooner S and Gersch H A 1971 *AIP Conf. Proc.* **5** 1334
[3] Alikhanov R A 1959 *Sov. Phys.–JETP* **36** 1204
[4] Kanamori J 1958 *Prog. Theor. Phys.* **20** 890
[5] Dove M T, Hagen M, Harris M J, Powell B M, Steigenberger U and Winkler B 1992 *J. Phys.: Condens. Matter* **4** 2761
[6] Cowley R A 1987 *Methods of Experimental Physics* vol 23, part C (New York: Academic) p 18
[7] Collins M F 1989 *Magnetic Critical Scattering* (Oxford: Oxford University Press)
[8] Lynn J W, Mook H A and Buyers W J L 1975 *Phys. Rev.* B **12** 238
[9] Hagen M 1994 The PRISMA GENIE data analysis programs *Rutherford Appleton Laboratory Report* 94-086
[10] Payne S J 1994 *MPhil Thesis* Keele University
[11] Hagen M and Payne S J 1995 A guide to critical scattering measurements using time of flight neutron diffraction *Rutherford Appleton Laboratory Report* RAL-TR-95-034
[12] Tucciarone A, Lau H Y, Corliss L M, Delapalme A and Hastings J M 1971 *Phys. Rev.* B **4** 3206
[13] Hagen M and Steigenberger U 1992 *Nucl. Instrum. Methods Phys. Res.* B **72** 239
[14] Bevington P R and Robinson D K 1995 *Data Reduction and Error Analysis for the Physical Sciences* 2nd edn (London: McGraw-Hill)
[15] Cooper M J and Nathans R 1967 *Acta Crystallogr.* **23** 357
[16] Werner S A and Pynn R 1971 *J. Appl. Phys.* **42** 4736